Three-body fragmentation mechanism of $C_2H_4^{3+}$ produced by 18-keV/u Ne^{8+} impact

Baihui Ren,[1] Zihan Xia,[1] Yu Zhang,[2,*] Long Wei,[1] Wandong Yu,[3] Jie Han,[1] Bo Wang,[1] Yaming Zou,[1] Li Chen,[1] and Baoren Wei[1,†]

[1]*Institute of Modern Physics, Key Laboratory of Nuclear Physics and Ion-Beam Application (MOE), Fudan University, Shanghai 200433, China*

[2]*College of Data Science, Jiaxing University, Jiaxing 314001, China*

[3]*State Key Laboratory for Mesoscopic Physics, Frontiers Science Center for Nano-optoelectronics, School of Physics, Peking University, Beijing 100871, China*

(Received 10 May 2021; accepted 15 July 2021; published 12 August 2021)

In this article we present the three-body fragmentation dynamics of $C_2H_4^{3+}$ caused by 18-keV/u Ne^{8+} ion impact. Utilizing the cold target recoil ion momentum spectroscopy, the complete kinematical information of three fragmentation channels, i.e., $C_2H_4^{3+} \rightarrow H^+ + H^+ + C_2H_2^+$, $H^+ + CH^+ + CH_2^+$, and $H^+ + H_2^+ + C_2H^+$ is obtained. For each channel, both concerted and sequential fragmentation mechanisms are observed and differentiated through the momentum correlation of resultant fragments visualized by the Dalitz plot and the Newton diagram. In particular, for the channel $C_2H_4^{3+} \rightarrow H^+ + H^+ + C_2H_2^+$, it is found in addition to the sequential pathway that the two protons can be emitted concertedly in two ways, i.e., from the same carbon atom or from the two carbon atoms. The present results show a more diverse molecular fragmentation triggered by ion collisions in contrast to a previous study using intense laser field ionization.

DOI: 10.1103/PhysRevA.104.022811

I. INTRODUCTION

The investigation of fragmentation processes of polyatomic molecules is a fundamental aspect in physical science and closely related to the plasma physics, interstellar chemistry, and other research areas [1–3]. When excited by the interaction with different particles, the molecule can proceed with different fragmentation patterns including two-body, three-body, or other more complicated dissociation processes. The three-body fragmentation, which is the subject of the present paper, usually involves two or more bonds breaking finally leading to three fragments and has recently attracted much more attention [4–12]. Various fragmentation mechanisms with distinct dynamics, e.g., concerted and sequential fragmentation, asymmetric bond stretching, and bond bending prior to the bond cleavage, have been identified in the three-body fragmentation of triatomic molecules, e.g., CO_2 [4–7], N_2O [8], OCS [9,10], and CS_2 [11,12].

Organic hydrocarbon molecules, e.g., CH_4, C_2H_2, and C_2H_4 exist widely in the universe (e.g., as the constituent of planetary atmospheres [2,3]) and play an important role in our daily life and industry. Those molecules have more than three nuclei, and their fragmentation is expected to be more complicated after exposure to different ionization fields. The concerted and sequential breakings of C–H bonds have been analyzed in the three-body fragmentation of CH_4 [13–15] and C_2H_2 [16–21] induced by photoionization or charged particle collisions. When the C–C bond cleavage is further involved, much more fragmentation pathways take place as observed in the dissociation of C_3H_4 trications [22–24]. Ethylene is one of the smallest hydrocarbons with a planar structure, and more hydrogen atoms might mean more ways to produce hydrogen species when it fragments. Therefore, it could serve as a prototype to study the fragmentation patterns of much more complex molecules. However, only a few works have reported the three-body fragmentation process of ethylene [25,26]. Xie *et al.* [25] have investigated the fragmentation mechanism of two dissociation channels, i.e., $H^+ + H^+ + C_2H_2^+$ and $H^+ + CH^+ + CH_2^+$ of $C_2H_4^{3+}$ produced by intense laser ionization. One concerted and one sequential pathway were identified for the former channel, whereas two sequential pathways were identified for the latter one. In the concerted process, it was found that the two nonadjacent C–H bonds broke simultaneously, and the heavier $C_2H_2^+$ moiety was almost still. In general, the triple ionization caused by an intense laser field occurs usually through a sequential ionization involving valence electrons, whereas the direct ionization in the Coulomb field from the highly charged ion (HCI) could react on both outer and inner electrons [27]. Therefore, a different molecular fragmentation scenario and more fragmentation pathways could happen under HCI collisions.

In this paper, we use 18-keV/u Ne^{8+} impact to initiate the three-body fragmentation of $C_2H_4^{3+}$. Taking advantage of a cold target recoil ion momentum spectroscopy (COLTRIMS) setup [28], we focus on the fragmentation dynamics of channels $C_2H_4^{3+} \rightarrow H^+ + H^+ + C_2H_2^+$ and $C_2H_4^{3+} \rightarrow H^+ + CH^+ + CH_2^+$ and another novel channel with the formation of H_2^+, $C_2H_4^{3+} \rightarrow H^+ + H_2^+ + C_2H^+$. By analyzing the momentum correlation of three fragments displayed in the Dalitz plot [29,30] and the Newton diagram [31,32], the

*zyclay@outlook.com
†brwei@fudan.edu.cn

fragmentation mechanism (concerted and/or sequential) in each dissociation channel will be identified. In the pathway identification, simulations via the Coulomb explosion model (CEM) for the concerted process and Dalitz plot for the sequential process are performed.

II. EXPERIMENTAL METHOD

The experiments were carried out on a COLTRIMS setup in conjunction with a 150-kV HCI collision platform at Fudan University. A detailed description can be found in our previous publications [15,21], and only a brief introduction is given here. A beam of 18-keV/u Ne^{8+} ions ($v = 0.85$ a.u.) produced from an electron cyclotron resonance ion source crossed with the supersonic jet of ethylene gas in a high vacuum collision chamber. After the interaction, the recoil ionic fragments resulting from the fragmentation of molecular ions were extracted and accelerated by the uniform electrostatic field of 100 V/cm and then fled through the field-free drift tube onto a position sensitive detector (PSD) equipped with two microchannel plates and a delay-line anode. The axis of the time-of-flight (TOF) tube is perpendicular to both the directions of the ion beam and the supersonic jet. The scattered projectiles with different charge states caused by charge exchange were separated by an electrostatic deflector and finally detected by another PSD. The coincidence signal of scattered and recoil ions served as the trigger of the multihit time-to-digital convertor.

Ion species were identified by the TOF spectra, and dissociation channels were distinguished by the corresponding coincidence TOF map. Finally, the three-dimensional (3D) momentum vectors of recoil ions were reconstructed from the TOF and position in the PSD. Additionally, according to the momentum vectors of recoil ions, the fragmentation dynamics of concerned fragmentation channels were deduced. The measurements were calibrated by the Coulomb explosion kinematics of N_2 dication under the same experimental condition. The random coincidence events were largely excluded by adopting a strict momentum conservation constraint during data analysis, i.e., the momentum sum of three coincidence fragments is limited to lie between ±5 a.u..

The Dalitz plot and Newton diagram are useful tools for revealing the molecular dissociation mechanism by visualizing the momentum vector relations [4]. In a Dalitz plot, the experimental data are placed inside a circle inscribed in an equilateral triangle. The distance from the data point to the edge i of the triangle is the relative squared momentum ε_i of the ith fragment. The ε_i values of three fragments are normalized and calculated by the following formula:

$$\varepsilon_i = p_i^2 \Big/ \sum_i p_i^2, \tag{1}$$

where p_i is the momentum value of the ith fragment. In a Newton diagram, the momentum of the first fragment is represented by an arrow with a size of 1 arbitrary unit along the horizontal axis. The momenta of the second and third fragments are normalized to the first fragment's momentum and placed in the upper and lower halves of the plot. It should be noted that in the present paper the three-body fragmentation channels of ethylene trications are analyzed with no selection on the final charge states of the scattered projectile ions.

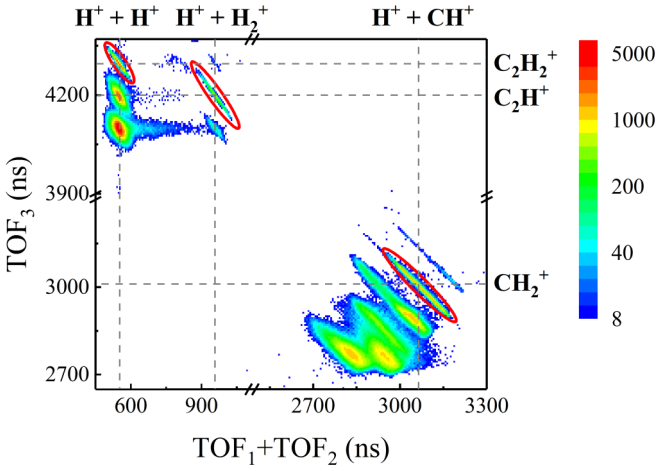

FIG. 1. Triple-ion coincidence TOF map of the $C_2H_4^{3+}$ ions caused by the 18-keV/u Ne^{8+} impact.

III. RESULTS AND DISCUSSION

Figure 1 shows a part of the triple-ion coincidence TOF map for the fragmentation of $C_2H_4^{3+}$ trications induced by 18-keV/u Ne^{8+} ion collisions. The horizontal axis is the sum of the TOFs of the first and the second detected ions, and the TOF of the third fragment ion is along the vertical axis. The intense islands with different slopes correspond to various dissociation channels of three- or many-body fragmentation of the precursor $C_2H_4^{q+}$ ($q \geqslant 3$). The structures surrounded by red elliptic lines are identified to result from the complete three-body fragmentation of $C_2H_4^{3+}$, which will be discussed in this article and named as fragmentation channels I–III as follows:

$$C_2H_4^{3+} \rightarrow H^+ + H^+ + C_2H_2^+, \quad \text{(I)}$$

$$C_2H_4^{3+} \rightarrow H^+ + CH^+ + CH_2^+, \quad \text{(II)}$$

$$C_2H_4^{3+} \rightarrow H^+ + H_2^+ + C_2H^+. \quad \text{(III)}$$

In fragmentation channel I, two protons and a heavier $C_2H_2^+$ moiety are produced following the breaking of two C–H bonds. Channel II is a fragmentation process with the cleavage of both C–H and C–C bonds. Besides bond breaking, bond formation is also involved in channel III as the recombination of the H–H bond is required to form H_2^+. The relative branching ratio for channel I is estimated as ∼66%, which is significantly larger than ∼29% and ∼5% for channels II and III, respectively. To ensure the complete collection of ionic fragments and avoid the influence of the dead time of the detector, the angle between the momentum of H^+ and the TOF axis is limited to be smaller than 40° in each channel. On this basis, the above branching ratios have a margin of error of about 15%, mainly due to the detection efficiency and statistical errors. In the following subsections, we will analyze the fragmentation mechanism of the three channels according to the momentum correlation of resultant fragments.

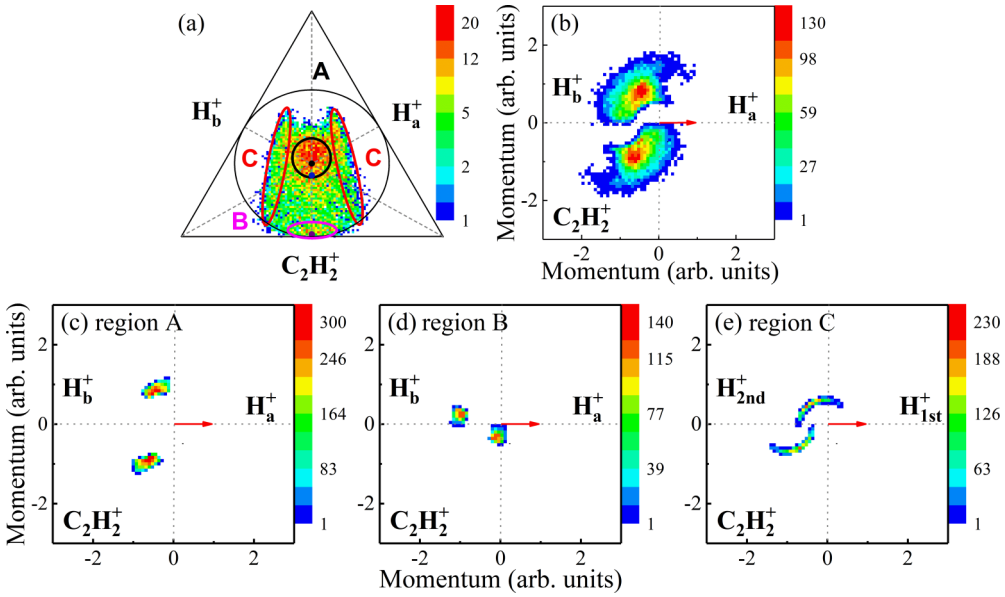

FIG. 2. (a) The Dalitz plot of fragmentation channel I. Intense areas are surrounded by black, magenta, and red ellipse lines and marked as A–C, respectively. The black, blue, and purple dots on the vertical middle line are momentum correlation patterns calculated by the Coulomb explosion model. H_a^+ presents the first detected proton, and H_b^+ is the second one. (b) Newton diagram of fragmentation channel I. The momentum of H_a^+ is taken as the unit vector, indicated by a red arrow, the relative momentum vectors of H_b^+ and $C_2H_2^+$ are mapped in the upper and lower halves of the plot. (c)–(e) Newton diagrams with Dalitz filters A–C, respectively. In (e) H_{1st}^+ and H_{2nd}^+ represent the protons produced in the first and second steps of the corresponding sequential fragmentation process.

A. Fragmentation channel $H^+ + H^+ + C_2H_2^+$

Channel I with two C–H bonds breaking could result from the following concerted or sequential fragmentation pathways:

$$C_2H_4^{3+} \rightarrow H^+ + H^+ + C_2H_2^+, \quad \text{(Ia)}$$

$$C_2H_4^{3+} \rightarrow H^+ + C_2H_3^{2+} \rightarrow H^+ + H^+ + C_2H_2^+. \quad \text{(Ib)}$$

To elucidate the fragmentation dynamics in detail, the Dalitz plot and Newton diagram are plotted in Figs. 2(a) and 2(b). As shown in Fig. 2(a) the data points are placed in a circle. And the three sides of the equilateral triangle represent fragment ions, i.e., two H^+ (denoted as H_a^+ and H_b^+) and residual $C_2H_2^+$. The distance between a data point and one of the sides, e.g., H_a^+, represents the relative squared momentum of H_a^+. There are two intense areas located at the middle and the bottom of the vertical dashed line marked as regions A and B, respectively. The events distributed in a / \ shape are surrounded by two red ellipse lines, marked as region C. Such multiple data structures indicate complex fragmentation mechanisms responsible for channel I.

Figure 2(b) shows the Newton diagram of channel I. The red arrow fixed at unit 1 represents the momentum vector of the first detected proton H_a^+, the momentum vectors of the second proton H_b^+ and the $C_2H_2^+$ ion are normalized to H_a^+ and placed above and below the x axis, respectively. Only two clearly concentrated intense areas can be identified in Fig. 2(b). To more clearly distinguish the various fragmentation mechanisms existing in channel I, Newton diagrams with different Dalitz filters of regions A–C are displayed in Figs. 2(c)–2(e), respectively. Due to the conservation of momentum, the 3D momentum vectors of dissociation products should be particular values for a concerted fragmentation process [33,34]. In Fig. 2(a), the data points located within region A are clustered near the center of the triangle, and the vertical distances to the three edges are very close, indicating that the momenta of the H_a^+, H_b^+, and $C_2H_2^+$ ions are comparable. The corresponding Newton diagram shown in Fig. 2(c) presents two islandlike structures, showing narrow momentum distributions of H_b^+ and $C_2H_2^+$. Those features indicate that a concerted fragmentation process leads to region A. The angles between two islands and the unit arrow represent the angles between the momentum vectors of H_b^+ / $C_2H_2^+$ and H_a^+. As shown in Fig. 3, the measured angle between momentum vectors of H_b^+ and H_a^+ is distributed from 90 ° to 140 ° and that of $C_2H_2^+$ and H_a^+ is in the range of 100 °–140 °. Gaussian fitting is performed on the above

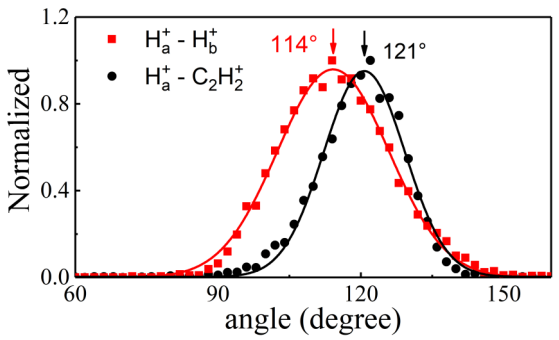

FIG. 3. Distribution of the angle between momentum vectors of H_a^+ and H_b^+ (red squares) and that of H_a^+ and $C_2H_2^+$ (black circles) of the concerted fragmentation in region A of channel I. The red and black curves are the Gaussian-fitting results.

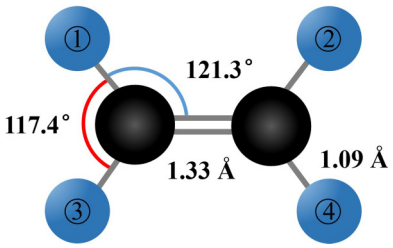

FIG. 4. Chemical structure of the neutral ethylene molecule.

two angular distributions and the peak values are ∼114 ° and ∼121 °, respectively.

In Fig. 2(a), region B is also a concentrated area and distributed at the bottom of the vertical middle line near the $C_2H_2^+$ edge where the momentum of $C_2H_2^+$ ion is around zero and the momenta of H_b^+ and H_a^+ are approximately equal. In the corresponding Newton diagram of Fig. 2(d), the momentum distributions of H_b^+ and $C_2H_2^+$ ions are concentrated around points (−1,0) and (0,0), which further confirms that the two protons are likely to be emitted back to back leaving the $C_2H_2^+$ ion almost at rest. Thus, the fragmentation events in region B result from another concerted fragmentation process, and the angle between momentum vectors of two protons is near 180 °.

Two concerted fragmentation processes are observed with rather different momentum distributions, which might be a result of the unique molecular structure of ethylene demonstrated in Fig. 4. There are four identical hydrogen atoms which are marked as ①–④ for convenience. Different combinations of two emitted protons during a concerted fragmentation process, e.g., ①②, ①③, and ①④, can result in different momentum distribution patterns. According to Fig. 3, the momentum angle between two protons in region A is around 114 °, thus, they might be distributed on positions ①② or ①③. If the protons are emitted in opposite directions from positions ①④, under such Coulomb repulsion the middle $C_2H_2^+$ ion will be left with negligible translational kinetic energy. This is more likely the case shown in Fig. 2(d) where the angle between momentum vectors of H_b^+ and H_a^+ is close to 180 °.

To further confirm the dissociation mechanisms of regions A and B, the point-charge CEM [35] is applied to calculate momentum vectors of the fragments in different concerted processes. In the calculation, the fragment is considered as a point-charge particle, which possesses mass and charge located at the center of mass. The initial structural parameters, e.g., bond length and bond angle, of $C_2H_4^{3+}$ are assumed consistent with the equilibrium configuration of the neutral ethylene molecule as shown in Fig. 4. The coordinate and momentum of each fragment are then obtained by numerically solving the classical motion equations in a Coulomb field. The calculated momentum vectors were normalized by formula (1) and represented by three dots • in Fig. 2(a). The black, blue, and purple dots located on the vertical middle line from top to bottom correspond to the momentum correlation patterns of proton combinations ①③, ①②, and ①④, respectively. Corresponding angles between the momentum vectors of H_a^+ and H_b^+ are calculated to be 119 °, 127 °, and 180 °, respectively.

Comparing the experimental data in Fig. 2(a) with the results of CEM calculations, two noteworthy features can be obtained. First, the angle of two protons in region A is around 114 °, which is close to 119 ° represented by the top black dot, and smaller than 127 ° represented by the blue dot in the middle. Therefore, the top black dot which represents the fragmentation combination ①③, is most likely to be the main contribution of the concerted fragmentation process in region A. But the existence of fragmentation combination ①② cannot be ruled out completely. Since the initial structure of $C_2H_4^{3+}$ may be slightly rearranged before fragmentation which deviates from the planar structure of C_2H_4, the present measurement accuracy is not enough to effectively distinguish proton combinations ①③ and ①②. Second, the momentum correlation pattern of fragments in region B is in good agreement with the bottom purple dot. This indicates that the concerted fragmentation mechanism in region B is mainly contributed by the two protons emitted from positions ① and ④.

In Fig. 2(a) for the /\-shaped region C, a similar structure has been observed in a previous experiment of C_2H_2 [20] as caused by a two-step sequential process. The first detected proton H_a^+ can be the proton produced in either the first or the second step (labeled as H_{1st}^+ and H_{2nd}^+, respectively), which leads to the symmetric /\ shape. The Newton diagram is plotted in Fig. 2(e), the momentum distributions of H_{2nd}^+ and $C_2H_2^+$ ions are represented by two semicircular structures, which is a typical feature of a two-step sequential dissociation. In the first step, the precursor $C_2H_4^{3+}$ dissociates into the intermediate $C_2H_3^{2+}$ and fragment H_{1st}^+. After rotation, the intermediate ion dissociates into the final products $C_2H_2^+$ and H_{2nd}^+ in the second step. The intensity of semicircular distribution decreases with the decrease in the angle (H_{1st}^+ vs H_{2nd}^+) and cutoff at ∼50 °, which implies that the lifetime of the intermediate $C_2H_3^{2+}$ is less than its rotation period, leading to the fragmentation occurring before a complete rotation. In such a two-step dissociation, $C_2H_4^{3+} \rightarrow H_{1st}^+ + C_2H_3^{2+} \rightarrow H_{1st}^+ + H_{2nd}^+ + C_2H_2^+$, the momentum of H_{1st}^+ is almost independent of the second step, which is consistent with the result observed in the Dalitz plot. The mass ratio of the second step fragments H_{2nd}^+ and $C_2H_2^+$ is 1/26. This leads to a large divergence of their momenta inherited from the parent ion $C_2H_3^{2+}$ and, thus, results in a far distance between the centers of the two semicircular structures in the Newton diagram in Fig. 2(e). Besides, the events outside the area of regions A–C may be attributed to the deformation of molecular structure of $C_2H_4^{3+}$, e.g., molecular bending and asymmetric stretching of chemical bonds as described in Ref. [4].

The two fragmentation mechanisms identified for the events in the regions B and C were also identified in the three-body fragmentation of $C_2H_4^{3+}$ caused by intense laser ionization [25]. Compared to the former study, a remarkable difference here is the occurrence of the concerted fragmentation process corresponding to region A with different C–H bond breaking, i.e., the two protons are emitted concertedly from the same carbon atom. The difference may be attributed to the different ionization mechanisms of laser field and ion collision. The dissociative ionization induced by laser pulse carries out sequentially in the outermost orbital, i.e., the

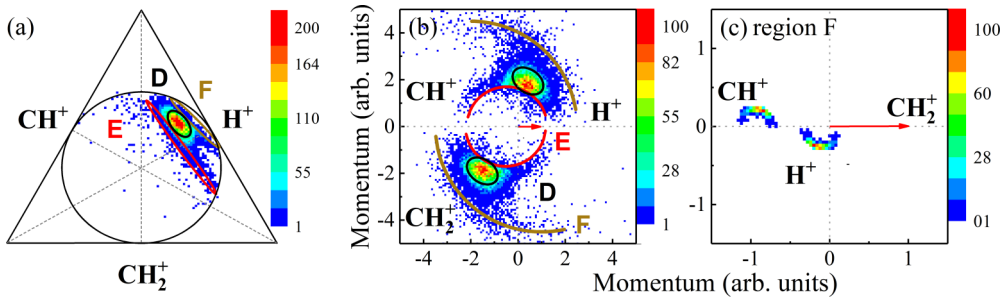

FIG. 5. (a) The Dalitz plot of fragmentation channel II. The fragmentation events located at different regions are marked by D–F, corresponding to different fragmentation mechanisms. (b) The Newton diagram of channel II. The momentum of fragment H^+ is set as a unit vector and plotted at the horizontal axis as a red arrow. The momenta of fragments CH^+ and $CH_2{}^+$ are plotted at the upper and lower halves. The structures marked by black, red, and golden lines correspond to the fragmentation events in regions D–F in Fig. 6(a), respectively. (c) The Newton diagram for the data in region F. The momentum of fragment $CH_2{}^+$ is set as the unit vector.

neutral C_2H_4 is stripped off two electrons in the first step, then the doubly charged $C_2H_4{}^{2+}$ ion is excited and ionized to the $C_2H_4{}^{3+}$ ion to dissociate into the final fragments. Although in the collisions of HCIs the direct ionization is dominant which might relate to electrons in more inner orbitals, and this might lead to different fragmentation pathways [27,36].

B. Fragmentation channel $H^+ + CH^+ + CH_2{}^+$

Figures 5(a) and 5(b) present the Dalitz plot and Newton diagram of the fragmentation channel II. As can be seen, there are three momentum correlation patterns marked as regions D–F, respectively. The gathering island structure in region D is a typical feature of concerted fragmentation process, which is located at the upper right side of the Dalitz plot, indicating that the momenta of CH^+ and $CH_2{}^+$ are much larger than the momentum of the proton. In Fig. 5(b), the momentum angle between fragments CH^+ and H^+ is significantly smaller than the angle between $CH_2{}^+$ and H^+, which is consistent with the chemical structure shown in Fig. 4. The corresponding pathway for the concerted fragmentation process is as follows:

$$C_2H_4{}^{3+} \rightarrow H^+ + CH^+ + CH_2{}^+, \quad \text{(IIa)}$$

which is also a newly reported dissociation pathway compared to the laser-induced work [25].

In a sequential fragmentation process, the momentum distributions of the ions produced in the second Coulomb explosion process are no longer related to the Coulomb field in the first step. Thus, the stripelike regions E and F in the Dalitz plot might be attributed to the following two-step sequential fragmentation processes:

$$C_2H_4{}^{3+} \rightarrow H^+ + C_2H_3{}^{2+} \rightarrow H^+ + CH^+ + CH_2{}^+, \quad \text{(IIb)}$$

$$C_2H_4{}^{3+} \rightarrow CH_2{}^+ + CH_2{}^{2+} \rightarrow H^+ + CH^+ + CH_2{}^+. \quad \text{(IIc)}$$

The distribution of region E is parallel to the H^+ side, that is, the momentum of the proton is independent of the momentum variations of CH^+ and $CH_2{}^+$, which indicates that the fragmentation results from the two-step sequential process IIb. The proton is emitted in the first step, and then the $C_2H_3{}^{2+}$ dissociates to CH^+ and $CH_2{}^+$ ions. When the momentum vector of the CH^+ fragment obtained in the second Coulomb explosion fragmentation is parallel, perpendicular, or antiparallel to the vector of the intermediate $C_2H_3{}^{2+}$, the corresponding fragmentation events are located at the bottom, middle, or top of the region B in Fig. 5(a). In Fig. 5(b), the two semicircular structures marked by red lines also indicate a sequential fragmentation mechanism with a proton emitted in the first step. However, the distribution of region F in the Newton diagram marked by golden lines is too diffuse to identify corresponding mechanism. Thus, we plot the Newton diagram where the unit vector is set to the momentum of $CH_2{}^+$ for region F in Fig. 5(c). There are two identifiable semicircle structures indicating that fragment $CH_2{}^+$ is the product of the first step, and H^+ and CH^+ ions are, subsequently, produced in the second step. Thus, it is confirmed that the fragmentation in region F corresponds to a sequential fragmentation process IIc in which the C–C bond breaks first before the C–H bond breaking. The two sequential processes are consistent with the fragmentation mechanism reported in the previous work driven by the laser field [25].

C. Fragmentation channel $H^+ + H_2{}^+ + C_2H^+$

Channel III, $C_2H_4{}^{3+} \rightarrow H^+ + H_2{}^+ + C_2H^+$, is a three-body fragmentation process including, in addition to bond breaking, the formation of a H_2 bond. This is consistent with the low branching ratio of ~5% for channel III. However, in the previous laser irradiation experiments in Ref. [25], channel III was not observed. As discussed earlier, the ionization mechanism of laser field and ion collision is quite different. This indicates that channel III could result from the dissociation of a higher excited state of $C_2H_4{}^{3+}$ involving inner electron ionization. The $H_2{}^+$ ion could be formed in two ways, that is, the two hydrogen atoms could be from the same or different carbon atoms as discussed by Gaire *et al.* [37] for ethylene dication dissociation. However, such details of fragmentation dynamics cannot be extracted based only on the present experimental results. Quantum chemical calculations are further needed. Here we try to identify the fragmentation mechanism of this channel using the Dalitz plot and Newton diagram as shown in Figs. 6(a) and 6(b), respectively. In Fig. 6(a), the intense area surrounded by the black line is marked as region G, and the dispersed area is denoted as region K. As discussed in channels I and II, the concentrated region G is a signature of the concerted

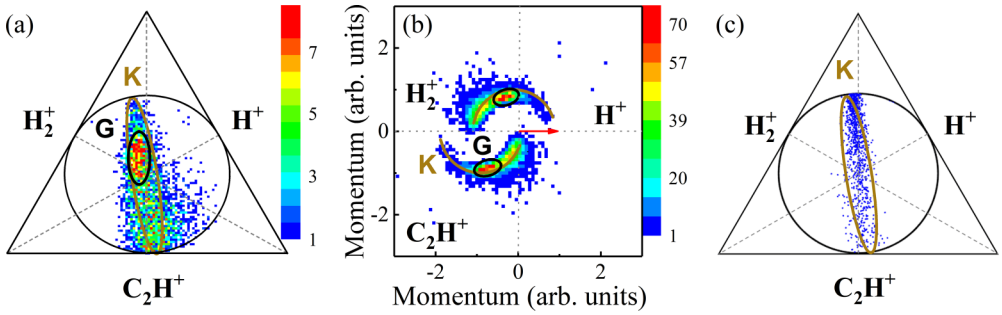

FIG. 6. (a) The Dalitz plot of fragmentation III. Two different momentum correlation patterns are marked by black and golden lines and denoted as regions G and K, respectively. (b) The Newton diagram of fragmentation III. The momentum of H^+ is set as unit vector. The momenta of fragments H_2^+ and C_2H^+ are plotted at the upper and lower halves. The structures marked by black and golden lines correspond to the fragmentation events in regions G and K in (a), respectively. (c) Simulated Dalitz plot for the sequential fragmentation pathway IIIb. The momenta of fragments are calculated by solving the kinetic equations in the sequential process.

fragmentation process,

$$C_2H_4{}^{3+} \rightarrow H^+ + H_2{}^+ + C_2H^+. \quad \text{(IIIa)}$$

Besides that, it can be seen that the bottom area of the Dalitz plot in Fig. 6(a) is slightly brighter than the middle area, inferring there might be another concerted fragmentation mechanism which is similar to the case of the fragmentation channel I. However, due to the lower statistics and overlap with region K, it is difficult to distinguish the second concerted process in both the Dalitz plot and the Newton diagram.

Region K marked by golden line is distributed in a striplike structure in Fig. 6(a) and in two semicircles in Fig. 6(b), which are strong evidences of a sequential fragmentation process. To more clearly identify it as shown in Fig. 6(c), a simulation of the Dalitz plot is performed for the following sequential fragmentation process:

$$C_2H_4{}^{3+} \rightarrow H^+ + C_2H_3{}^{2+} \rightarrow H^+ + H_2{}^+ + C_2H^+. \quad \text{(IIIb)}$$

In a pure sequential fragmentation process the first and second steps are independent of each other. The kinetic energy and momenta released in the first and second steps of channel IIIb are defined as E_1, $\vec{P}_{1st}$, and E_2, $\vec{P}_{2nd}$, respectively. Following the conservation of momentum, the momentum values of the fragments H^+, $H_2{}^+$, and C_2H^+ are calculated by following equations and then the Dalitz plot can be reconstructed

$$\vec{P}_1 = \vec{P}_{1st}, \quad (2)$$

$$\vec{P}_2 = -\frac{m_2}{m_2+m_3}\vec{P}_{1st} + \vec{P}_{2nd}, \quad (3)$$

$$\vec{P}_3 = -\frac{m_3}{m_2+m_3}\vec{P}_{1st} - \vec{P}_{2nd}, \quad (4)$$

where the m_i and $\vec{P}_i$ $(i = 1\text{–}3)$ represent the mass and momentum of the fragments H^+, $H_2{}^+$, and C_2H^+, respectively. The values of $\vec{P}_{1st}$ and $\vec{P}_{2nd}$ are defined to be $|\vec{P}_{1st}| = \sqrt{2E_1m_1(m_2+m_3)/(m_1+m_2+m_3)}$ and $|\vec{P}_{2nd}| = \sqrt{2E_2m_2m_3/(m_2+m_3)}$. E_1 and E_2 are set according to the present experiment results as Gauss(9.1, 1.0) and Gauss(4.5, 0.5), respectively. The Gauss(E,w) function represents a Gaussian distribution of which the center value is E and the full width at half maximum is w in eV. The angle between $\vec{P}_{1st}$ and $\vec{P}_{2nd}$ is distributed randomly between 0° and 180°. It can be seen that the simulation result is in good agreement with the feature of the region K in Fig. 6(a). Thus, the above sequential process IIIb is responsible for the formation of channel III.

IV. CONCLUSIONS

To summarize, the three-body fragmentation processes of $C_2H_4{}^{3+}$ induced by the 18-keV/u Ne^{8+} ion impact are investigated. With the aid of the COLTRIMS technique, three fragmentation channels (I) $H^+ + H^+ + C_2H_2{}^+$, (II) $H^+ + CH^+ + CH_2{}^+$, and (III) $H^+ + H_2{}^+ + C_2H^+$ are observed through the triple-ion coincidence TOF map. To identify the fragmentation mechanism involved in each channel, the Dalitz plot and Newton diagram displaying the momentum correlation of fragments are used. It is found that one sequential and two different concerted fragmentation processes are responsible for channel I. These two concerted processes showing different fragmentation kinematics, e.g., different momentum values of the $C_2H_2{}^+$ fragment, corresponds to different C–H bond cleavages, which are confirmed by the CEM simulation. Channel II is mainly attributed to a concerted fragmentation process and two sequential ones in which the C–C bond breaks first, and then the C–H bond breaks in the second step or vice versa. As for channel III involving bond breaking and formation, the concerted fragmentation process is also found playing a role. As the signatures for different pathways overlap largely in the experimental Dalitz plot or Newton diagram, a simulation of the Dalitz plot is performed, which confirms the existence of a sequential process, i.e., after the first step of proton emission, in the second step $H_2{}^+$ and C_2H^+ ions are formed.

Compared to the previous work of C_2H_4 ionization by strong laser field [25], some new pathways, e.g., the two protons are concertedly emitted from the same carbon site in channel I, are observed in the present paper. It indicates different molecular excitation and ionization effects caused by the intense laser field and Coulomb field of HCIs. To better understand the evolution or change in fragmentation mechanism in this channel, in addition to quantum chemical calculations, a series of experiments using HCIs of different velocities could be carried out, and questions, e.g., does the emission of two protons occur at the same carbon site or different sites, might be answered more thoroughly.

ACKNOWLEDGMENTS

This work was supported by the National Natural Science Foundation of China under Grants No. U1832201 and No. 11674067, the National Key Research and Development Program of China under Grant No. 2017YFA0402300, and by the Shanghai Leading Academic Discipline Project (Project No. B107).

[1] D. Reiter and R. K. Janev, Contrib. Plasma Phys. **50**, 986 (2010).
[2] W. D. Geppert and M. Larsson, Chem. Rev. **113**, 8872 (2013).
[3] D. K. Boehme, Phys. Chem. Chem. Phys. **13**, 18253 (2011).
[4] N. Neumann, D. Hant, L. P. H. Schmidt, J. Titze, T. Jahnke, A. Czasch, M. S. Schöffler, K. Kreidi, O. Jagutzki, H. Schmidt-Böcking, and R. Dörner, Phys. Rev. Lett. **104**, 103201 (2010).
[5] E. Wang, X. Shan, Z. Shen, M. Gong, Y. Tang, Y. Pan, K.-C. Lau, and X. Chen, Phys. Rev. A **91**, 052711 (2015).
[6] A. Khan, L. C. Tribedi, and D. Misra, Phys. Rev. A **92**, 030701(R) (2015).
[7] S. Srivastav, A. Sen, D. Sharma, and B. Bapat, Phys. Rev. A **103**, 032821 (2021).
[8] A. Khan, L. C. Tribedi, and D. Misra, Phys. Rev. A **96**, 012703 (2017).
[9] J. Rajput, T. Severt, B. Berry, B. Jochim, P. Feizollah, B. Kaderiya, M. Zohrabi, U. Ablikim, F. Ziaee, K. Raju P., D. Rolles, A. Rudenko, K. D. Carnes, B. D. Esry, and I. Ben-Itzhak, Phys. Rev. Lett. **120**, 103001 (2018).
[10] H. Kumar, P. Bhatt, C. P. Safvan, and J. Rajput, J. Chem. Phys. **148**, 064302 (2018).
[11] A. Hishikawa, H. Hasegawa, and K. Yamanouchi, Chem. Phys. Lett. **361**, 245 (2002).
[12] E. Wang, M. Gong, Z. Shen, X. Shan, X. Ren, A. Dorn, and X. Chen, J. Chem. Phys. **149**, 204301 (2018).
[13] I. Ben-Itzhak, K. D. Carnes, S. G. Ginther, D. T. Johnson, P. J. Norris, and O. L. Weaver, Phys. Rev. A **47**, 3748 (1993).
[14] R. Flammini, M. Satta, E. Fainelli, G. Alberti, F. Maracci, and L. Avaldi, New J. Phys. **11**, 083006 (2009).
[15] Y. Zhang, T. Jiang, L. Wei, D. Luo, X. Wang, W. Yu, R. Hutton, Y. Zou, and B. Wei, Phys. Rev. A **97**, 022703 (2018).
[16] N. Saito, M. Nagoshi, M. Machida, I. Koyano, A. De Fanis, and K. Ueda, Chem. Phys. Lett. **393**, 295 (2004).
[17] A. Hishikawa, A. Matsuda, M. Fushitani, and E. J. Takahashi, Phys. Rev. Lett. **99**, 258302 (2007).
[18] R. Flammini, M. Satta, E. Fainelli, and L. Avaldi, Phys. Rev. A **83**, 014501 (2011).
[19] S. De, J. Rajput, A. Roy, P. N. Ghosh, and C. P. Safvan, Phys. Rev. A **77**, 022708 (2008).
[20] S. Xu, X. L. Zhu, W. T. Feng, D. L. Guo, Q. Zhao, S. Yan, P. Zhang, D. M. Zhao, Y. Gao, S. F. Zhang, J. Yang, and X. Ma, Phys. Rev. A **97**, 062701 (2018).
[21] T. Jiang, B. Wang, Y. Zhang, L. Wei, S. Chen, W. Yu, Y. Zou, L. Chen, and B. Wei, Phys. Rev. A **100**, 022705 (2019).
[22] H. Xu, T. Okino, and K. Yamanouchi, J. Chem. Phys. **131**, 151102 (2009).
[23] H. Xu, T. Okino, and K. Yamanouchi, Appl. Phys. A: Mater. Sci. Process. **104**, 941 (2011).
[24] C. Ma, S. Xu, D. Zhao, D. Guo, S. Yan, W. Feng, X. Zhu, and X. Ma, Phys. Rev. A **101**, 052701 (2020).
[25] X. Xie, E. Lötstedt, S. Roither, M. Schöffler, D. Kartashov, K. Midorikawa, A. Baltuška, K. Yamanouchi, and M. Kitzler, Sci. Rep. **5**, 12877 (2015).
[26] B. Wang, L. Wei, Y. Zhang, W. Yu, Y. Zou, L. Chen, and B. Wei, J. Phys. B: At., Mol. Opt. Phys. **53**, 155205 (2020).
[27] E. Wang, X. Shan, L. Chen, T. Pfeifer, X. Chen, X. Ren, and A. Dorn, J. Phys. Chem. A **124**, 2785 (2020).
[28] R. Dörner, V. Mergel, O. Jagutzki, L. Spielberger, J. Ullrich, R. Moshammer, and H. Schmidt-Böcking, Phys. Rep. **330**, 95 (2000).
[29] R. H. Dalitz, Philos. Mag. (1798-1977) **44**, 1068 (1953).
[30] R. H. Dalitz, Phys. Rev. **94**, 1046 (1954).
[31] J. H. D. Eland, Mol. Phys. **61**, 725 (1987).
[32] S. Hsieh and J. H. D. Eland, J. Phys. B: At., Mol. Opt. Phys. **30**, 4515 (1997).
[33] P. Bhatt, T. Sairam, A. Kumar, H. Kumar, and C. P. Safvan, Phys. Rev. A **96**, 022710 (2017).
[34] S. K. Kim, S. Pedersen, and A. H. Zewail, J. Chem. Phys. **103**, 477 (1995).
[35] Y. Wang, X. Shi, J. Zhou, S. Xu, D. Guo, S. Yan, X. Zhu, and X. Ma, Phys. Rev. A **101**, 042706 (2020).
[36] B. Wales, R. Karimi, E. Bisson, S. Beaulieu, M. Giguère, T. Motojima, R. Anderson, J. Matsumoto, J.-C. Kieffer, F. Légaré, H. Shiromaru, and J. Sanderson, Phys. Scr. **2013**, 014068 (2013).
[37] B. Gaire, D. J. Haxton, F. P. Sturm, J. Williams, A. Gatton, I. Bocharova, N. Gehrken, M. Schöffler, H. Gassert, S. Zeller, J. Voigtsberger, T. Jahnke, M. Zohrabi, D. Reedy, C. Nook, A. L. Landers, A. Belkacem, C. L. Cocke, I. Ben-Itzhak, R. Dörner, and T. Weber, Phys. Rev. A **92**, 013408 (2015).